

Bayesian Machine Learning meets Formal Methods: An application to spatio-temporal data

LAURA VANA-GÜR, TU Wien, Austria

ENNIO VISCONTI*, TU Wien, Austria

LAURA NENZI, University of Trieste, Italy

ANNALISA CADONNA, University of Klagenfurt, Austria

GREGOR KASTNER, University of Klagenfurt, Austria

We propose an interdisciplinary framework that combines Bayesian predictive inference, a well-established tool in Machine Learning, with Formal Methods rooted in the computer science community. Bayesian predictive inference allows for coherently incorporating uncertainty about unknown quantities by making use of methods or models that produce predictive distributions, which in turn inform decision problems. By formalizing these decision problems into properties with the help of spatio-temporal logic, we can formulate and predict how likely such properties are to be satisfied in the future at a certain location. Moreover, we can leverage our methodology to evaluate and compare models directly on their ability to predict the satisfaction of application-driven properties. The approach is illustrated in an urban mobility application, where the crowdedness in the center of Milan is proxied by aggregated mobile phone traffic data. We specify several desirable spatio-temporal properties related to city crowdedness such as a fault-tolerant network or the reachability of hospitals. After verifying these properties on draws from the posterior predictive distributions, we compare several spatio-temporal Bayesian models based on their overall and property-based predictive performance.

CCS Concepts: • Mathematics of computing → Bayesian computation; • Software and its engineering → Formal software verification; • Computing methodologies → Model verification and validation.

Additional Key Words and Phrases: Bayesian predictive inference, spatio-temporal models, formal verification methods, posterior predictive verification, urban mobility

1 INTRODUCTION

Formal verification methods have a long-standing tradition in the computer science community. They have historically emerged in the context of hardware and software systems to provide strong guarantees about the correctness of the analyzed implementation by verifying the satisfaction of complex logical properties. From deterministic systems, formal verification methods have found plenty of applications in stochastic systems, where the same set of inputs can correspond to multiple sets of random outputs. The traditional approach to formal verification of stochastic systems is probabilistic model checking [introduced independently by 10, 32]. However, in the context of very large stochastic systems, numerical probabilistic model checking is practically infeasible [36], and new approaches have been developed, such as Statistical Model Checking (SMC) [see 22, for a recent survey on the area], which is a simulation-based version of probabilistic model checking. The idea of SMC is to calculate the probability of satisfaction of logical properties by Monte Carlo integration, that is, simulate many trajectories from the stochastic system, determine for each trajectory if the logical property is satisfied, and take the arithmetic mean over the number of simulations. Given the parallelizable nature of SMC, the computational bottleneck becomes the simulation and verification of a complex logical property at each iteration. Here, formal methods come into play: complex properties are translated into logical formulae, which can then be automatically verified using

*Corresponding author

Authors' addresses: Laura Vana-Gür, laura.vana.guer@tuwien.ac.at, TU Wien, Vienna, Austria; Ennio Visconti, ennio.visconti@tuwien.ac.at, TU Wien, Vienna, Austria; Laura Nenzi, University of Trieste, Trieste, Italy; Annalisa Cadonna, University of Klagenfurt, Klagenfurt, Austria; Gregor Kastner, gregor.kastner@aau.at, University of Klagenfurt, Klagenfurt, Austria.

efficient algorithms tailored to the type of logic employed. The primary advantage of specifying properties as logic formulae comes from the efficient monitoring algorithms that are available to automatically check whether the specified properties are satisfied or not, and to which extent. Given its scalability, SMC has therefore become increasingly used in different application domains, especially related to biological systems and cyber-physical systems [see 30, for an application of a continuous-time Markov chain model to model a bike sharing system].

SMC applications usually consider the model parameters to be fixed to specific values (e.g., the maximum likelihood estimates) and simulate from the stochastic system conditioned on the fixed parameter values, without taking into account how the uncertainty on the parameter naturally propagates to the satisfaction probability. While there are extensions to SMC to include prior information about the probability of the satisfaction of a property, such as Bayesian SMC [37], the finite set of trajectories remains simulated from a model with fixed parameter values. On the opposite side, to deal with such uncertainty, [5–7] consider directly the parameters as uncertain and calculate the probability of satisfaction for a set of possible parameter combinations. However, while the range of the parameters was determined based on prior knowledge, the values of the parameters are not estimated based on observed data.

In this paper, we propose a Bayesian Machine Learning approach that naturally deals with uncertainty propagation, while simultaneously it allows to learn the value of the parameters from the data. Our proposed approach extends the classical approach to SMC to a Bayesian framework by performing verification and monitoring on trajectories of the Bayesian predictive distribution drawn using the MCMC algorithm employed for model estimation. Bayesian predictive inference allows the coherently accounting for uncertainty about an unknown or future value of the random variable being modeled by providing the entire posterior predictive distribution. This novel framework provides a unifying approach to the modeling and statistical analysis of data that coherently accounts for the uncertainty of the specified properties.

While we believe a Bayesian approach to uncertainty can enrich SMC, we also argue that the use of Formal Methods in the (Bayesian) Machine Learning community opens the door for interesting application-driven methods for prediction and model evaluation and comparison. In most applications, predictions are obtained from a (Bayesian) Machine Learning model which are then compared to the observed data in order to assess the model performance ex-post (i.e., post-estimation). However, predictions obtained from a (Bayesian) Machine Learning model are not directly translated into a decision but rather transformed, compressed, and combined with further rules or requirements relevant to the decision problem at hand. As a simple example, consider an algorithmic trading scheme using a predictive model for stock returns, which will use the output of the predictive model together with the rule “place a sell order if the 90% quantile of the predictive stock return distribution exceeds 10% three days in a row”. Or a traffic officer who will decide to divert traffic if the model predicts crowdedness to rise above a certain threshold along the city’s main arteries. Such rules could also be employed to put monitoring systems in place for the predictive models (especially black-box ones); e.g., for the purpose of ensuring fairness in the predictions. Especially in high-dimensional, complex models, these requirements or properties relevant for decision-making are typically highly nonlinear functions of the random variables, and one is interested in their predictive distribution. Their verification ex-ante as well as their evaluation ex-post (as part of the posterior model checking and comparison exercise) could provide valuable insights to the modeler and decision-maker and could tailor the analysis to the concrete needs of the decision problem. We claim that the focus should be placed on application- and decision-specific requirements or properties that the system being modeled should satisfy also when evaluating and comparing the performance of different Machine Learning models.

We achieve this by leveraging an existing stream of literature in the computer science field of SMC and verification to approximate the posterior predictive probability of satisfaction of these properties, as well as a posterior predictive measure of property reliability or robustness. We then introduce the Bayesian predictive probability of satisfaction and posterior predictive robustness as quantities of interest and show how these measures can be used for comparing a collection of spatio-temporal Bayesian models. This property-related comparison can complement common predictive evaluation measures such as the log predictive density scores.

We demonstrate our novel approach with spatio-temporal areal data, where measurements are collected over time at various areal units, and a neighboring matrix allows calculating the distance between the different units. In particular, we consider an urban mobility application, given that urban population density dynamics are highly variable both in space and time. For such applications, building a Bayesian spatio-temporal model that accurately predicts future population dynamics, is of paramount importance to decision-makers in the context of urban planning (e.g., who must plan for resource allocation, divert traffic and increase mobile network capabilities temporarily) but has far-reaching implications related to the environment, economy, and health [14]. In particular, the latter link became even more evident in the context of the COVID-19 pandemic. Analyzing mobile phone traffic data as a proxy for population mobility has been widely employed in the past years [e.g., 3, 11, 14, 31, and references therein], with applications ranging from population density estimation in the absence of census data [35] to traffic prediction [e.g., 18] and to modeling the spread of epidemics [e.g., 4, 9]. Given the high dimensionality of mobile phone data, only a few studies have focused on sophisticated (Bayesian) modeling tools in an urban planning context. [8] build a spatio-temporal model with spatial clustering of the locations in Milan using data from an Italian telecommunications company; [34] conducted an empirical study in Shenzhen, China where they include the population statistics and indices for mixed-use to explore the spatial pattern of population fluctuation in a Bayesian model.

For illustration purposes, we employ in this work open source data from the “Telecom Italia Big Data Challenge”, which contains telecommunications activity aggregated over a fixed spatial grid of the city of Milan during the months of November and December 2013. Our results provide a deeper understanding of urban dynamics in Milan in terms of the best-performing model which identifies clusters of areas with similar temporal patterns and in terms of when and how well the formulated properties are satisfied.

The paper is organized as follows: Section 2 introduces the concept of formal verification for spatio-temporal data, together with new application-specific properties. Section 3 explains how the Bayesian predictive framework allows for the incorporation of uncertainty. Section 3.2 proposes measures for predictive evaluation in terms of property satisfaction. The empirical data and results are presented in Section 4. Section 5 concludes and outlines directions for future work.

2 FORMAL VERIFICATION FOR AREAL SPATIO-TEMPORAL DATA

2.1 Introduction to STREL logic

With the goal of incorporating application-specific properties into the Bayesian Machine Learning workflow, we introduce formal verification methods as a way to specify and verify such properties. A formal verification method has the goal of checking whether a (stochastic) system satisfies some properties or requirements, which are stated in some formal language. The last decade has seen a great effort to develop logic-based specification languages and monitoring frameworks for spatio-temporal properties; in our case, we consider STREL [27] as the specification language of reference. A spatio-temporal logic combines atomic propositions via a set of operators: the standard Boolean operators (\vee , \neg , \rightarrow , ...), temporal operators to specify the temporal evolution and spatial

operators to reason about the space. Let us describe the language more in detail and how it can be applied to spatio-temporal data.

In our application, we consider a grid of $i = 1, \dots, I$ areas, which covers the center of the city of Milan, where a measurement of crowdedness y is collected over time at $t = 1, \dots, T$, where one time-point represents a time interval of 10 minutes. The distance between two areal units i and j is the path that minimizes the number of “hops” or “jumps” from cell i to cell j . This distance can be calculated by using a symmetric neighboring matrix, where the entry at row i and column j (and vice versa), is 1 if areas i and j are adjacent, and 0 otherwise. While the framework is rather general, we are primarily interested in the properties in a predictive context. Thus, we will formulate and consider requirements on the future crowdedness values up to h -steps ahead of a given time t . Each requirement that we formulate can be checked for every areal unit $i = 1, \dots, I$. The logic formulae are then specified with the language generated by the following grammar, which defines rules for building formulae recursively starting from the atomic proposition:

$$\varphi := \mu \mid \neg \varphi \mid \varphi_1 \wedge \varphi_2 \mid F_{\leq h} \varphi \mid G_{\leq h} \varphi \mid \varphi_1 R_{\leq d} \varphi_2 \mid E_{\leq d} \varphi. \quad (1)$$

The atomic propositions μ in STREL are defined for a location i and time s and they can describe the indexes (e.g., whether location i contains a hospital or whether s corresponds to midnight) or they can be defined as inequalities on the relevant variables (in our application city crowdedness) e.g., $y_{i,s} > c_{i,s}$ or $y_{i,s} < c_{i,s}$ for $c_{i,s} \in \mathbb{R}$. Note that the quantities entering the atomic propositions are univariate and that the logic cannot, at the time of writing, express inequalities of the form e.g., $y_{i,s} > y_{i,s-1} + c_{i,s}$. The logical operators then combine different truth values of atomic propositions $\mathbb{1}(\mu_{i,s}) \in \{0, 1\}$ for a sequence of locations and time points, i.e., $\forall (i, s)$ in an index set Λ . Boolean operators like \neg and \wedge denote the classical negation and conjunction. We use $F_{\leq h} \varphi$ and $G_{\leq h} \varphi$ as the *eventually* and *always* temporal operators, respectively. The former denotes the occurrence of property φ at least *once* in the future time interval $(t, t+h]$, while the latter checks the occurrence of property φ in *all* future time points in the interval $(t, t+h]$ (for discretely observed systems, a constant behavior in between time points is assumed). When the context requires also lower bounds to the times of interest, we will adopt an interval-based notation, like $F_{[a,b]}$, to denote the interval $[t+a, t+b]$. Lastly, spatial operators are represented by the reach $\varphi_1 R_{\leq d} \varphi_2$ and escape $E_{\leq d} \varphi$ operators for a distance $d \in \mathbb{R}^+$. The former represents the *reachability* of an area where φ_2 holds by only passing through locations that satisfy φ_1 where the total distance of the path should be at most d . The latter operator describes the possibility of *escaping* from a certain location via a route passing only through locations that satisfy φ , with the distance between the starting location of the path and the last being at most d . Moreover, other operators such as disjunction \wedge , implication \rightarrow , or further spatial operators can be derived. One example is the *somewhere* operator $\Diamond_{\leq d} \varphi$ which checks whether there exists a location that satisfies φ reachable via a route with a distance of at most d .

Once the properties are specified as logic formulae, efficient algorithms tailored to the type of logic employed are available to approximate the behavior of the stochastic system with respect to the properties. One is interested firstly in property satisfaction $S_i(\mathbf{y}_{t+1:h}, \varphi)$, i.e., whether the quantities of interest satisfy property φ for area i , considering the time period between $t+1$ and $t+h$. It should be noted that the satisfaction of spatial properties in the area i will depend not only on the values of crowdedness in i for the time period of interest, but also on the values in other areas. STREL provides a Boolean monitoring algorithm for this purpose, which returns a yes/no answer while checking for the satisfaction of a given logical formula on a specific realization from the system. Secondly, one also wants to quantify the reliability of a property. This is measured by the robustness function $R_i(\mathbf{y}_{t+1:h}, \varphi)$, which is defined as the bound on the perturbation that the quantities of interest can tolerate without changing the truth value of a property [12]. The

quantitative monitoring algorithm of STREL computes the value of the robustness function for a given realization. There is a soundness property between the Boolean and the quantitative monitoring such that a positive value corresponds to satisfaction and a negative value to violation of the property. The robustness function is defined recursively on the operators of the logic [see 27], starting from the atomic proposition. For the atomic proposition, e.g., $\mu_{i,s} = y_{i,s} > c_{i,s}$, the robustness is given by the difference between the quantity of interest $y_{i,s}$ and the threshold value $c_{i,s}$.

We refer the interested reader to [27] for a complete and formal description of the logic, or to [28] for a more practice-oriented list of case studies. We devote the rest of this section to highlighting the key benefits of adopting the STREL machinery for property verification. The primary advantage is that STREL is a specification language crafted specifically for keeping a strong connection with intuitive notions of spatial and temporal concepts, allowing to express complex requirements in a compact and understandable way. Note that a dedicated scripting language for STREL is available. It allows expressing the formulae in almost plain English. Moreover, a key advantage of specifying requirements in terms of STREL operators is that the open-source software Moonlight [29] is readily available for automatically verifying that a given set of predictions satisfies the provided specification. Lastly, the automatic monitoring of STREL specification implemented by Moonlight takes into account state-of-the-art algorithms for maximizing memory and computational time efficiency (with usually better performances than alternatives). While ad-hoc algorithms can be more efficient if they are tailored to a given specification, they are often costly to adapt as the monitored properties evolve. Therefore, the generality offered by the framework and the Moonlight software ensures easy adaptability of the property specifications with minimal changes from the modeler.

2.2 Crowdedness requirements

2.2.1 Informal specification of requirements. In this section, we propose some informal properties that the crowdedness level in a big city should satisfy to robustly withstand critical events. Let c represent a crowdedness threshold for all the areas of the city. Note, however, that the framework can accommodate for, e.g., area-specific threshold values. We restrict ourselves to a universal c for the sake of simplicity in the exposition. This threshold would typically be known to the decision-maker and would correspond to the maximum value for which a certain location would still be considered uncrowded. Moreover, let h_φ be a time step in the future to be used in a property or requirement φ .

One possible stakeholder of our proposed framework is a telecommunications company, which would like to have a predictive alert system to ensure that their mobile network does not get over-crowded. The following three properties could be of interest to the telecommunications company:

- P.1** *Overloads are temporary*: if the level of crowdedness goes above the threshold c in the period following t , then it must return below c latest by time $t + h_{P.1}$.
- P.2** *Overloads are local*: if at a certain location the level of crowdedness at $t + h_{P.2}$ rises above c , this location must be at most at distance $d_{P.2}$ from another location with a level of crowdedness below c at the same time. This is a minimal spatial requirement for a city grid trying to balance excessive loads.
- P.3** *The network is fault-tolerant*: for a location, the level of crowdedness in that location or in other locations within a distance of $d_{P.3}$ should be below c at all times in the interval $(t, t + h_{P.3}]$, i.e., emergency load-balancing must be possible.

In addition to the previous requirements that are related to general aspects of the mobile network, for the evaluation of the city in terms of safety and quality of life, it is interesting to look at how the

city is performing with respect to the reachability of some key points of interest. For example, in an emergency scenario, a traffic monitoring body would be interested in the following requirement (assuming that our crowdedness measure is indeed a proxy for population density in the city):

P.4 Uncrowded reachability: A hospital must be reachable within a distance of $d_{P.4}$ from any uncrowded location of the city center, in the time interval $(t, t + h_{P.4}]$, by only going through uncrowded locations.

2.2.2 Formalizing the requirements. We show here how to use the STREL logic presented in Section 2.1 to specify the requirements introduced above. The previous requirements will be in the following formally expressed as STREL formulae, and the key operators will be described gradually. Before looking at the formalization of the requirements, we introduce the atomic property,

$$\phi = (y > c),$$

i.e., the crowdedness is above a certain threshold c . Conversely, the formula $\neg\phi$ represents the case where the crowdedness level is below or equal the threshold c . This formula constitutes the basic building block for formalizing our requirements; in fact, the first requirement is related to temporary overloads, which can be formulated by using temporal operators in the following way:

$$\varphi_{P.1} = \phi \rightarrow F_{\leq h_{P.1}} \neg\phi. \quad (P.1)$$

The second property, related to overloads being local, can be formalized as a spatio-temporal property:

$$\varphi_{P.2} = F_{=h_{P.2}} (\phi \rightarrow \diamondsuit_{\leq d_{P.2}} \neg\phi). \quad (P.2)$$

Note that the temporal operator $F_{=h_{P.2}}$ here denotes that the requirement shall hold at the time which lies $h_{P.2}$ -steps ahead in the future.

Thirdly, the fault-tolerance of the network is a spatio-temporal requirement, which can be formulated as

$$\varphi_{P.3} = G_{\leq h_{P.3}} (\diamondsuit_{\leq d_{P.3}} \neg\phi), \quad (P.3)$$

where $G_{\leq h_{P.3}}$ requires the “somewhere” property to hold globally for the whole interval $(t, t + h_{P.3}]$.

Lastly, for the requirement related to the reachability of hospitals, let us first introduce a new atomic proposition:

$$\phi_2 = isHospital.$$

Here, ϕ_2 is a peculiar proposition representing hospital locations, meaning that it is satisfied only when the current location comprises a hospital. A first, direct translation of the P.4 could be the following:

$$F_{\leq h_{P.4}} (\neg\phi \mathcal{R}_{\leq d_{P.4}} \phi_2).$$

While the previous requirement formalizes P.4 *literally*, it likely gives an unrealistic interpretation of the requirement. In fact, $\neg\phi \mathcal{R}_{\leq d_{P.4}} \phi_2$ means that a hospital can be reached by only traversing uncrowded areas, however, it does not consider the traveling time to reach the location, meaning that the property would be satisfied *whenever* there is an uncrowded path to the hospital (although the actual traveling time might be significantly higher). A more realistic (although a bit more involved) version is presented below:

$$\varphi_{P.4} = \psi_{0,d_{P.4}}, \quad (P.4)$$

$$\psi_{i,n} = \begin{cases} \phi_2 & n = 0, \\ \phi_2 \vee \left((G_{[i,i+1]} \neg \phi) \wedge (\Diamond_{\leq 1} \psi_{i+1,n-1}) \right) & \text{otherwise.} \end{cases}$$

Property $\varphi_{P,4}$, with a slight abuse of notation, encodes our requirement and shows the flexibility of the logic approach. The requirement states that one needs to move at most $d_{P,4}$ cells in the time interval $(t, t + h_{P,4}]$ time units, but it does not explicitly specify how fast one can move through the different cells of the city grid. To give a realistic interpretation of the specification, we assumed that in one time unit (i.e., 10 minutes), one can only travel from one cell to the next. This interpretation translates into $\psi_{j,n}$, which imposes that the current location is not crowded for the next ten minutes, and iteratively enforces this n times by the recursive check of $\psi_{j,n}$ until the maximum distance is reached (in terms of “hops” on the grid), in which case it looks for a hospital in the neighborhood. This way, analyzing the satisfaction or robustness of $\varphi_{P,4}$, will not only provide insights about the spatial reachability of a hospital, but it will also take into account the traversal time needed to reach it.

3 PREDICTIVE MODEL CHECKING AND MODEL COMPARISON USING FORMAL METHODS

3.1 Incorporating uncertainty through the Bayesian approach

Our application aims to study the behavior of city crowdedness observed at regular time intervals on a fixed grid area. Again, let $y_{i,j}$ denote the crowdedness measure in area i at time j for $i = 1, \dots, I$ areal units on a city grid and $j = 1, \dots, T$ time points. As a framework for predictive inference, we assume the observations up to time $t < T$ are used as a training sample and the evaluation is performed on the observations at the remaining $t+1, \dots, T$ discrete time points. By using STREL, we are interested in investigating two functions or statistics of future crowdedness, namely the property satisfaction and the property robustness. To extend the concept of satisfaction and robustness over the whole stochastic system, we introduce two key concepts: i) the Bayesian predictive probability of satisfaction and ii) the expected value of the Bayesian predictive robustness.

As mentioned in the introduction, traditional SMC considers the parameters of the model fixed, generates a large number of trajectories from the model and then considers how many times the trajectories satisfy a given property. In the Bayesian framework, the parameters are not fixed but are given a prior distribution based on expert knowledge or prior observations. After observing the data, one then obtains a posterior probability distribution for the model parameters. We now show how we use the Bayesian approach to account for uncertainty on the parameters when calculating the probability of satisfaction and the robustness of a property. We start by introducing the Bayesian predictive density. The h -step ahead Bayesian predictive density is given by

$$p(\mathbf{y}_{t+h} | \mathbf{y}_{1:t}^o) = \int_{\mathcal{K}} p(\mathbf{y}_{t+h} | \mathbf{y}_{1:t}^o, \boldsymbol{\kappa}) p(\boldsymbol{\kappa} | \mathbf{y}_{1:t}^o) d\boldsymbol{\kappa}, \quad (2)$$

where $\mathbf{y}_{1:t}^o$ denotes the observed values up to time t of random variables $\mathbf{y}_{1:t} = (\mathbf{y}_1, \dots, \mathbf{y}_t)$ (each \mathbf{y}_i being I dimensional), $\boldsymbol{\kappa}$ contains all parameters and latent quantities to be estimated in the model, $p(\boldsymbol{\kappa} | \mathbf{y}_{1:t}^o)$ denotes their posterior distribution and \mathcal{K} contains the corresponding integration space. It can be seen that the predictive density in Equation (2) is given by the integral of the likelihood function, where the values of the unobservables $\boldsymbol{\kappa}$ are weighted according to their posterior distribution. This means that this predictive density integrates uncertainty about the vector of unobservables and the intrinsic uncertainty about the future value \mathbf{y}_{t+h} given the history $\mathbf{y}_{1:t}^o$. The posterior distribution $p(\boldsymbol{\kappa} | \mathbf{y}_{1:t}^o)$ can, in our proposed models, be accessed by generating M draws $\boldsymbol{\kappa}_{1:t}^{(m)}$ from the posterior up to time t using MCMC. The predictive distribution in Equation (2)

can then be accessed by simulating $\mathbf{y}_{t+h}^{(m)}$ from each of the distributions represented by the density $p(\mathbf{y}_{t+h}|\mathbf{y}_{1:t}^o, \boldsymbol{\kappa}_{1:t}^{(m)})$ for $m = 1, \dots, M$.

Starting from the predictive distribution, we can now define the Bayesian h -step-ahead predictive probability of satisfaction for property φ at location i and time t by

$$\begin{aligned} \mathbb{E}[S_i(\mathbf{y}_{t+1:h}, \varphi)|\mathbf{y}_{1:t}^o] &= \\ \int_{\mathbf{y}_{t+1} \in \mathcal{Y}_1} \dots \int_{\mathbf{y}_{t+h} \in \mathcal{Y}_h} S_i(\mathbf{y}_{t+1:h}, \varphi) p(\mathbf{y}_{t+1:h}|\mathbf{y}_{1:t}^o) d\mathbf{y}_{t+1} \dots d\mathbf{y}_{t+h}. \end{aligned} \quad (3)$$

We can avoid the calculation of the multidimensional integral in Equation 3 and approximate the probability by using the draws from the Bayesian predictive density,

$$\mathbb{E}[S_i(\mathbf{y}_{t+1:h}, \varphi)|\mathbf{y}_{1:t}^o] \approx \frac{1}{M} \sum_{m=1}^M S_i(\mathbf{y}_{t+1:h}^{(m)}, \varphi), \quad (4)$$

where for one draw m the $S_i(\mathbf{y}_{t+1:h}^{(m)}, \varphi)$ takes either value zero or value one.

The Bayesian predictive robustness is a function of the relevant predictions for the property φ together with the property parameters. For each location i and time t we can obtain a distribution of this measure by integrating over the posterior distribution of the unknowns. One can then look at summary statistics of this distribution, such as the expected value at location i and time t , which is given by

$$\begin{aligned} \mathbb{E}[R_i(\mathbf{y}_{t+1:h}, \varphi)|\mathbf{y}_{1:t}^o] &= \\ \int_{\mathbf{y}_{t+1} \in \mathcal{Y}_1} \dots \int_{\mathbf{y}_{t+h} \in \mathcal{Y}_h} R_i(\mathbf{y}_{t+1:h}, \varphi) p(\mathbf{y}_{t+1}, \dots, \mathbf{y}_{t+h}|\mathbf{y}_{1:t}^o) d\mathbf{y}_{t+1} \dots d\mathbf{y}_{t+h}, \end{aligned} \quad (5)$$

and can be approximated by

$$\mathbb{E}[R_i(\mathbf{y}_{t+1:h}, \varphi)|\mathbf{y}_{1:t}^o] \approx \frac{1}{M} \sum_{m=1}^M R_i(\mathbf{y}_{t+1:h}^{(m)}, \varphi). \quad (6)$$

Note, however, that also other summary statistics of the distribution could be employed for decision-making. For example, if a more conservative approach is desired, one can consider higher quantiles (e.g., 90%) of the posterior distribution of the robustness.

The monitoring algorithms of STREL are employed here to efficiently calculate (4) and (6) from the $m = 1, \dots, M$ posterior predictive draws. We note that both $S(\mathbf{y}_{t+1:h}, \varphi)$ and $R(\mathbf{y}_{t+1:h}, \varphi)$ can be seen as summary statistics in the sense of the classical posterior predictive model check [PPC, 15]. In our case, unlike in classical PPC, the summary statistics do not depend on the model parameters, but rather on the property parameters which are kept fixed throughout the analysis. The satisfaction is a binary statistic, while the robustness is continuous. Methods such as Bayesian p-values [15] can be employed on these statistics for the purpose of model evaluation.

3.2 Property-driven model comparison

The Bayesian predictive distribution in Equation (2) can also be employed for the purpose of model comparison by using the h -steps ahead log predictive density scores [cf. 16, 19]. If we evaluate (2) at the observed value \mathbf{y}_{t+h}^o , the h -step ahead LPDS is the real number:

$$\text{LPDS}_{t+h} = \log \int_{\mathcal{K}} p(\mathbf{y}_{t+h}^o|\mathbf{y}_{1:t}^o, \boldsymbol{\kappa}) p(\boldsymbol{\kappa}|\mathbf{y}_{1:t}^o) d\boldsymbol{\kappa} \approx \log \left(\frac{1}{M} \sum_{m=1}^M p(\mathbf{y}_{t+h}^o|\mathbf{y}_{1:t}^o, \boldsymbol{\kappa}_{1:t}^{(m)}) \right).$$

The LPDS evaluates a predictive model based only on the density value at the realizing outcome. However, it is not the only metric that can be employed for evaluating the predictive performance of probabilistic forecasts. Other scores can be employed depending on which forecast feature is desirable for the application at hand. For example, another commonly employed score which also rewards predictive distributions that place mass close to the realizing outcome is the continuous-ranked probability score [CRPS; 24]. More generally, these scores are sample estimates based on the observed data of scoring rules employed to measure prediction accuracy [17]. For a review of the estimation of scoring rules based on MCMC output, see [21].

We propose that, in addition to the above methods well-established in the Bayesian Machine Learning community, model assessment and comparison should be enhanced with considerations specifically tailored for the application at hand, and that they should take into account how the predictions from the Machine Learning model are used for decision making. This is why in the following we propose several measures that rely on the posterior predictive satisfaction and robustness of the properties introduced in Section 3.1.

In particular, we compare the posterior predictive satisfaction and robustness measures estimated on the M trajectories with the ex-post evaluation of the satisfaction and robustness of the properties on the observed data after time t $\mathbf{y}_{t+1:h}^o$. We compute for the following measures:

- Mean accuracy between the observed and estimated satisfaction,

$$\bar{\text{Acc}}_t^{\text{Satisf}} = \frac{1}{M} \sum_{m=1}^M \left(\frac{1}{I} \sum_{i=1}^I 1\{S_i(\mathbf{y}_{t+1:h}^{(m)}, \varphi) = 1\} 1\{S_i(\mathbf{y}_{t+1:h}^o, \varphi) = 1\} \right).$$

- Mean F1 score between the observed and estimated satisfaction,

$$\bar{\text{F1}}_t^{\text{Satisf}} = \frac{1}{M} \sum_{m=1}^M 2 \frac{\text{recall}^{(m)} \times \text{precision}^{(m)}}{\text{recall}^{(m)} + \text{precision}^{(m)}},$$

where

$$\begin{aligned} \text{precision}^{(m)} &= \frac{\sum_{i=1}^I 1\{S_i(\mathbf{y}_{t+1:h}^{(m)}, \varphi) = 1\} 1\{S_i(\mathbf{y}_{t+1:h}^o, \varphi) = 1\}}{\sum_{i=1}^I 1\{S_i(\mathbf{y}_{t+1:h}^{(m)}, \varphi) = 1\}}, \\ \text{recall}^{(m)} &= \frac{\sum_{i=1}^I 1\{S_i(\mathbf{y}_{t+1:h}^{(m)}, \varphi) = 1\} 1\{S_i(\mathbf{y}_{t+1:h}^o, \varphi) = 1\}}{\sum_{i=1}^I 1\{S_i(\mathbf{y}_{t+1:h}^o, \varphi) = 1\}}. \end{aligned}$$

- Root mean squared error (RMSE) between the observed and the estimated robustness,

$$\text{RMSE}_t^{\text{Rob}} = \sqrt{\frac{1}{M} \sum_{m=1}^M \left\{ \frac{1}{I} \sum_{i=1}^I (R_i(\mathbf{y}_{t+1:h}^{(m)}, \varphi) - R_i(\mathbf{y}_{t+1:h}^o, \varphi))^2 \right\}}.$$

4 EMPIRICAL ILLUSTRATION

4.1 Data

To illustrate the proposed framework, we employ a data set containing telecommunications activity data derived from call detail records (CDRs) for the center of Milan, Italy over the period of one week in November 2013. The CDR data is a valuable proxy for population distribution and people's mobility habits [31], given the almost universal use of mobile phones, and has a high potential in researching the patterns in mobility at a high frequency in time and over a large spatial network. Mobile communication service providers generate a CDR whenever a device state changes either because of the user's actions (phoning, texting, browsing on the internet) or because of technical reasons (e.g., switching to a cell with a stronger signal in the cellular network).

The data set employed in this paper is a subset of the “Telecom Italia Big Data Challenge” open source database, which contains various geo-referenced, aggregated and anonymized datasets for the city of Milan and the Province of Trentino [for a detailed description, see 2]. The telecommunications activity data covers the period November 01, 2013, to December 16, 2013, and the CDR data provided is aggregated in both space and time. In the case of Milan, the city area is composed of a grid overlay of 1000 squares with the size of approximately 235m×235m with the CDRs being aggregated inside each square. Additionally, a temporal aggregation is performed in time slots of ten minutes. Information on the type of activity that generated the CDR is also provided in the database:

- SMS-in activity: activity proportional to the amount of received short message services (SMSs) inside a given grid square during a given time interval. A CDR is generated each time a user receives an SMS.
- SMS-out activity: activity proportional to the amount of sent SMSs inside a given grid square during a given time interval. A CDR is generated each time a user sends an SMS.
- Call-in activity: activity proportional to the number of received calls inside a given grid square during a given time interval. A CDR is generated each time a user receives a call.
- Call-out activity: activity proportional to the number of issued calls inside a given grid square during a given time interval. A CDR is generated each time a user issues a call.
- Internet traffic activity: number of CDRs generated inside a given grid square during a given time interval. A CDR is generated each time a user starts an Internet connection or ends an Internet connection. During the same connection, a CDR is generated if the connection lasts for more than 15 min or the user transfers more than 5 MB.

The data is further anonymized by dividing the true number of records in each category by a constant known to Telecom Italia, which hides the true number of calls, SMS and internet connections.

Sample description. We consider a subset of the Milan telecommunications activity dataset covering the period November 04, 2013 (Monday) to November 11, 2013 (Monday) with $T = 6 \times 24 \times 8 = 1152$. We further restrict our analysis to the central 21×21 grid (i.e., $I = 441$), where the center-most cell is the one containing the location of the Milan Duomo. This grid corresponds to an area of around 25km^2 . Moreover, we consider the sum of all the mobile phone activity measures (i.e., SMS-in, SMS-out, call-in, call-out and internet) as our measure of crowdedness. We use this aggregated measure because i) the phoning (call-in, call-out) and texting by SMS measures are rather sparse during the night, as people rarely call or text after midnight, ii) the modern use of cell phones relies much more on browsing the internet or on messaging apps which gained popularity around 2010. As such, considering the internet CDRs in addition to the other four can paint a more realistic picture of the crowdedness of a certain area.

Figure 1 contains the crowdedness measure averaged over the 10-minute time intervals for the whole analyzed period over the 21×21 grid. Areas with high levels of crowdedness are apparent in the central grid squares in the area surrounding the Milan *Duomo* (3) and in the upper center, where the two main stations are, namely (1) *Garibaldi Station* and (2) *Central Station*. On the other hand, lower activity grid squares such as the ones overlaid on a highly trafficked avenue on the right-hand side and right bottom corner of the map can be identified.

In order to illustrate the temporal behavior of the crowdedness measure, we present in Figure 2 the time-series of the grid units containing the three representative districts of (3) *Duomo*, (5) *Navigli* and (4) *Bocconi*. We observe a larger high activity in the area of (3) *Duomo* compared to the other two districts, which peaks around midday during the working days and in the early afternoon on the weekends. (5) *Navigli* on the other hand, which is a district famous for its different types of cafés, restaurants, bars and design shops, exhibits a more uniform behavior among the working

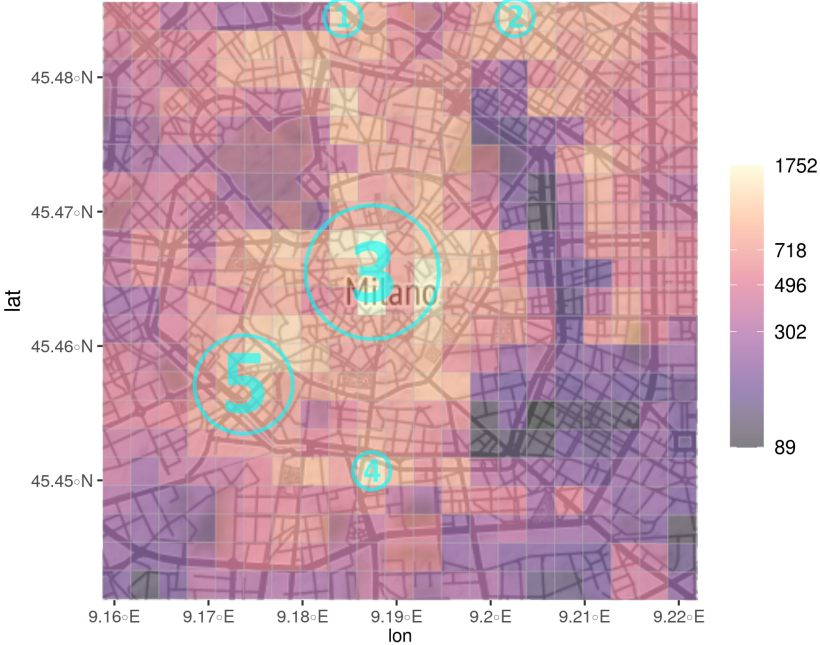


Fig. 1. Average crowdedness measure over the period November 04, 2013, to November 11, 2013. The x -axis contains the longitude and the y -axis contains the latitude degrees. The marked areas represent: (1) Garibaldi Station, (2) Central Station, (3) Duomo, (4) Bocconi, (5) Navigli.

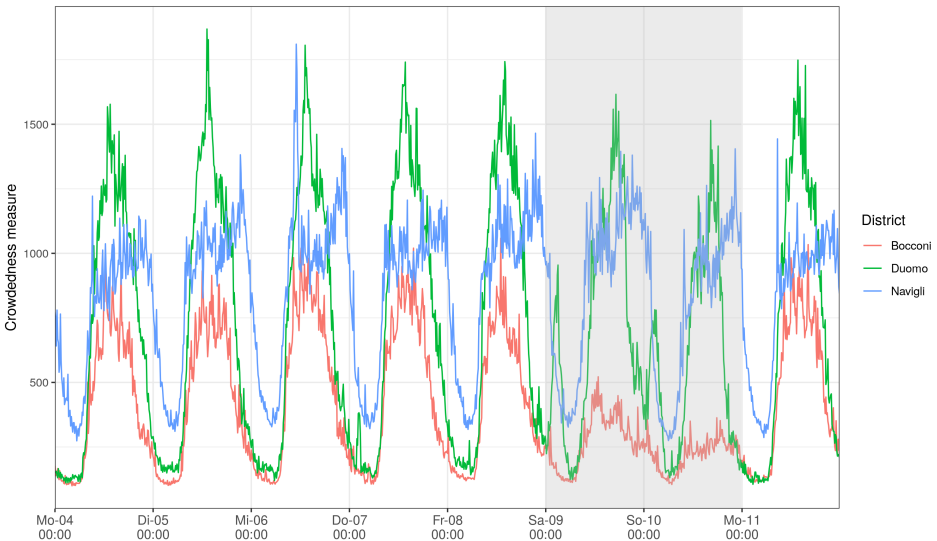


Fig. 2. Time series of the crowdedness measure for the areal units containing the districts Duomo, Navigli and Bocconi over the period from November 04, 2013, to November 11, 2013. Areas marked in gray represent weekends.

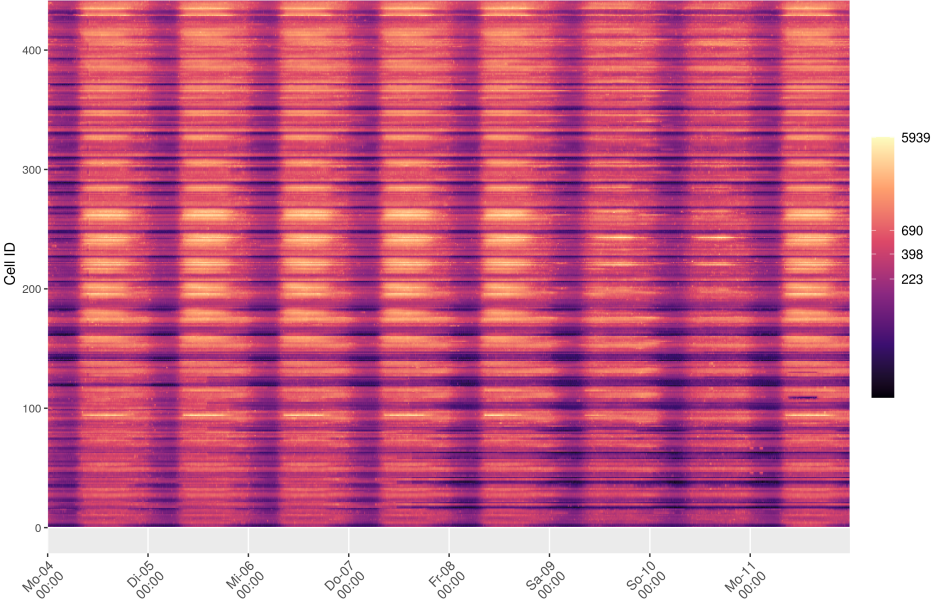


Fig. 3. Raster plot exhibiting the time series of the crowdedness measure for each of the 441 grid squares for the period November 04, 2013, to November 11, 2013.

and the weekend days, with activity peaking in the evening hours. The grid square containing the [\(4\)](#) *Bocconi* university exhibits a clear pattern during working hours and reduced activity levels on the weekends, especially on Sundays.

The seasonality in the data can be identified also in Figure 3, which contains a visualization of the whole dataset through a raster plot. Aside from the strong daily seasonality that is present in all locations, one can observe different temporal patterns among the areas. Most areas share the characteristic of relatively lower activity on the weekends, while the activity on the working days differs among groups of locations e.g., the locations from the central part of the grid (cell IDs 150–280) exhibit a higher difference between the daily crowdedness during working days vs. weekends, while locations with cell IDs around 400 (top cells in the map) exhibit rather similar activity during the workdays and weekends.

4.2 Model comparison

We employ in our analysis several Bayesian models to model the behavior of city crowdedness observed at regular time intervals on a fixed grid area. Let $y_{i,t}$ denote the crowdedness measure in area i at time t for $i = 1, \dots, I$ areas and $t = 1, \dots, T$ time points. As could be seen in descriptive figures, the measure exhibits seasonal behavior on both a daily and weekly level and this behavior is heterogeneous across the different areas. Similar to [8], we account for such characteristics in the model formulation by employing the following dynamic harmonic regression:

$$\log(y_{i,t}) = \beta_0 + \mathbf{h}_t^\top \boldsymbol{\beta}_i + \eta_{i,t},$$

where $\boldsymbol{\beta}_i$ is a vector of area-specific regression coefficients, $\eta_{i,t}$ is an error term and \mathbf{h}_t is a vector of dimension $2K$ of harmonic regressors [cf. 33].

$$\mathbf{h}_t = (\cos(2\pi\omega_{k_1} t), \sin(2\pi\omega_{k_1} t), \dots, \cos(2\pi\omega_K t), \sin(2\pi\omega_K t))^\top$$

where the term $\omega_k = k/T$ is a Fourier frequency for which the associated sinusoid completes an integer number of cycles in the observed length of time series, and K cannot be larger than $T/2$. In order to choose the dimension of the harmonic regressions, we inspect the estimated spectral densities of our $I = 21 \times 21 = 441$ time series (see Figure 4) and observe the strong intra-daily as well as an intra-weekly seasonality, with the largest values corresponding to 24-hour intervals. We use this information to select the 12 frequencies marked by vertical lines in Figure 4 in constructing the harmonic regression. This means that the dimension of our vector of covariates \mathbf{h}_t is 24.

Moreover, in order to capture the spatio-temporal dependence in crowdedness, the error term $\eta_{i,t}$ is split into two components:

$$\eta_{i,t} = w_{i,t} + e_{i,t},$$

where $e_{i,t}$ is normally distributed $e_{i,t} \stackrel{iid}{\sim} N(0, \sigma^2)$ and $w_{i,t}$ is a space-time random effect which captures the spatio-temporal dependence in the log crowdedness measure unexplained by the Fourier covariates.

In the following, we investigate and compare the predictive performance of different models for the random effects. As a baseline model, we consider a model with no random effects $w_{i,t} = 0$ and with one set of regression coefficients for all locations as the baseline. The most complex model we employ is one proposed in [8], where $w_{i,t}$ has a spatio-temporal specification and the area-specific coefficients β_i are clustered using a Bayesian non-parametric procedure (CAR-AR-BNP). This allows us to identify clusters of areas with similar temporal behavior while also keeping the model more parsimonious.

In addition to the CAR-AR-BNP model, we consider three CAR-AR models which all assume a common vector or regression coefficients for all areas with a normal prior: i) a model where the spatial auto-correlation parameter ρ is fixed to 0 (CAR-AR ($\rho = 0$)) – this only implies a temporal dependence structure, ii) a model where spatial auto-correlation parameter ρ is fixed to 0.5 (CAR-AR ($\rho = 0.5$)) – this only implies temporal dependence structure and a moderate spatial dependence, iii) a model where the spatial auto-correlation parameter ρ is estimated in the MCMC procedure (CAR-AR). More details about the models and the estimation procedure using MCMC can be found in Appendix A.

To evaluate the performance of the different models, we set up an out-of-sample exercise based on rolling windows, where we start by training the Bayesian model on data between November 04, 2013, at 00:00 (Monday) and November 10, 2013, 23:50 to generate one-, two- and three-step-ahead predictions, as well as for computing the predictive measures to be used for model selection for November 11, 2013, 00:00 up to November 11, 2013, 00:20. In a separate estimation procedure, we shift the window of the training data by 10 minutes and re-estimate the model in an iterative fashion until we reach the end of the sample.

All results are based on 10000 iterations of the Gibbs sampler, where the first 5000 are discarded as burn-in and the thinning parameter is set to 50. This leaves 100 draws to be used for inference. The number of draws is not as large as typical values, but we use it to keep the verification of the properties (especially for Property P.4) manageable in terms of computation time on a local computer. If one has access to a cluster of workstations, the number of iterations can be increased, as the property verification can trivially be parallelized. The trace plots of the models show acceptable convergence for all parameters, as well as good mixing.

Figure 5 presents the cumulative one-step ahead ($h = 1$) and three-step ahead ($h = 3$) log predictive Bayes factors for Monday, November 11, 2013:

$$\log \text{BF}_{t_1, t_2}(A, B) = \sum_{t=t_1}^{t_2-h} \log \text{LPDS}_{t+h}(A) - \log \text{LPDS}_{t+h}(B),$$

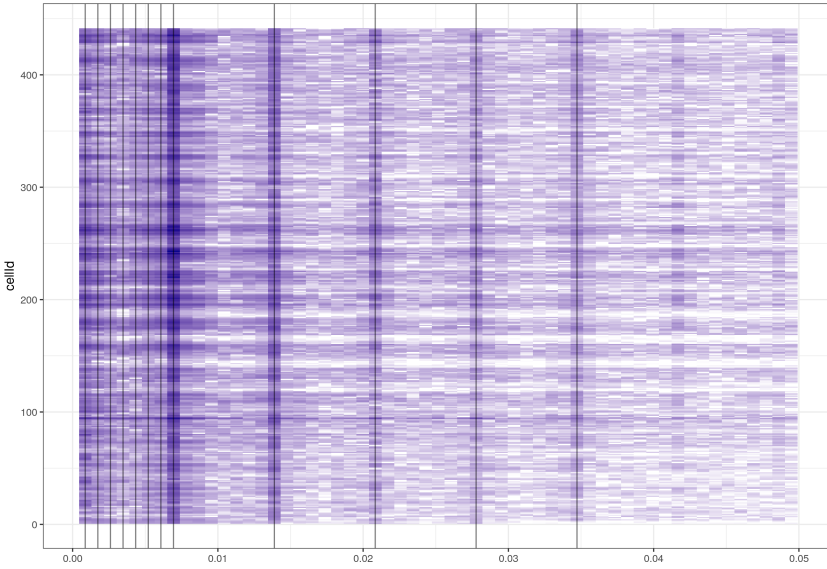


Fig. 4. Raster plot exhibiting the spectral density estimates for each of the 441 grid squares for the period from November 04, 2013, to November 11, 2013. The x -axis only exhibits frequencies up to 0.05. The black vertical lines represent the frequencies that were chosen to be included in the harmonic regression after visual inspection of this graph. The chosen frequencies correspond to the intra-weekly and intra-daily seasonality.

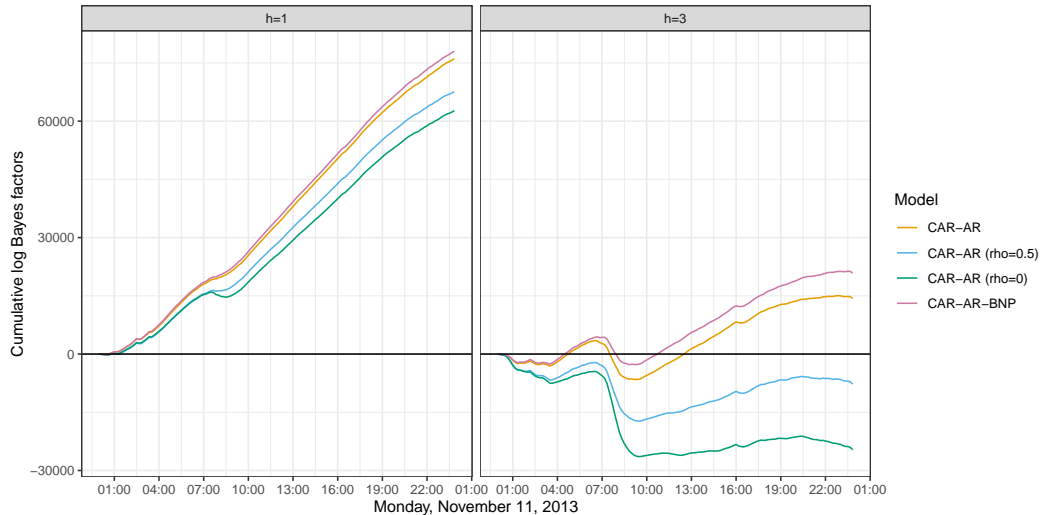


Fig. 5. One- and three-steps-ahead cumulative log predictive Bayes factors for different models relative to the baseline model.

where B is taken to be a baseline model. We observe that all models taking space and/or time correlation into account through the autoregressive structure outperform the baseline model, with the model CAR-AR-BNP with spatial clustering also outperforming, even if not by a lot, the CAR-AR model. In terms of the three-steps ahead prediction, the CAR-AR-BNP model is superior, but we

Table 1. Posterior means and standard deviations (in parentheses) of the predictive measures of accuracy and F1 scores for property satisfaction and the RMSE of the robustness for the four properties. The reported measures are averages over all test samples.

Measure	Baseline	CAR-AR $\rho = 0$	CAR-AR $\rho = 0.5$	CAR-AR	CAR-AR BNP
Property P.1					
\bar{Acc}^{Satisf}	0.6999 (0.0056)	0.944 (0.0025)	0.9479 (0.003)	0.9445 (0.0059)	0.9498 (0.0035)
$\bar{F1}^{Satisf}$	0.8027 (0.0029)	0.9555 (0.0019)	0.9584 (0.0022)	0.956 (0.0043)	0.9601 (0.0026)
$RMSE^{Rob}$	493.2178 (5.84)	101.979 (3.8052)	96.0108 (4.2172)	101.7701 (9.328)	92.9006 (6.104)
Property P.2					
\bar{Acc}^{Satisf}	0.8177 (0.0056)	0.9463 (0.0038)	0.9481 (0.0038)	0.9476 (0.0043)	0.9553 (0.0037)
$\bar{F1}^{Satisf}$	0.8988 (0.0033)	0.9678 (0.0022)	0.9688 (0.0023)	0.9686 (0.0025)	0.9731 (0.0022)
$RMSE^{Rob}$	273.7798 (8.4465)	59.9263 (2.771)	57.5646 (2.5964)	59.1099 (2.7259)	48.6895 (2.8436)
Property P.3					
\bar{Acc}^{Satisf}	0.9116 (0.0076)	0.9511 (0.0028)	0.9508 (0.0031)	0.9515 (0.0036)	0.9547 (0.0039)
$\bar{F1}^{Satisf}$	0.9439 (0.0051)	0.9692 (0.0018)	0.969 (0.0021)	0.9695 (0.0024)	0.9713 (0.0026)
$RMSE^{Rob}$	120.5187 (7.339)	59.3011 (1.9052)	59.1511 (2.8903)	58.645 (3.8598)	52.6133 (3.461)
Property P.4					
\bar{Acc}^{Satisf}	0.9268 (0.0061)	0.9703 (0.0034)	0.9722 (0.0037)	0.9726 (0.0043)	0.9743 (0.0034)
$\bar{F1}^{Satisf}$	0.8575 (0.0117)	0.939 (0.007)	0.9426 (0.0075)	0.9437 (0.0084)	0.947 (0.0068)
$RMSE^{Rob}$	280.6554 (20.4942)	130.225 (6.0651)	125.8994 (5.6114)	128.1106 (6.5048)	122.4351 (5.1467)

observe also that the performance of all CAR-AR models is worse than the baseline in the hours following midnight and between 07:00-09:00 (see negative slopes in the log Bayes factor curves). Furthermore, the gain in performance of the CAR-AR models diminishes around 19:00, when the slopes of the curves are not as steep. These results point towards the fact that there might be a change in the spatial dependence parameter ρ throughout the day. We leave such an extension of the model to further research.

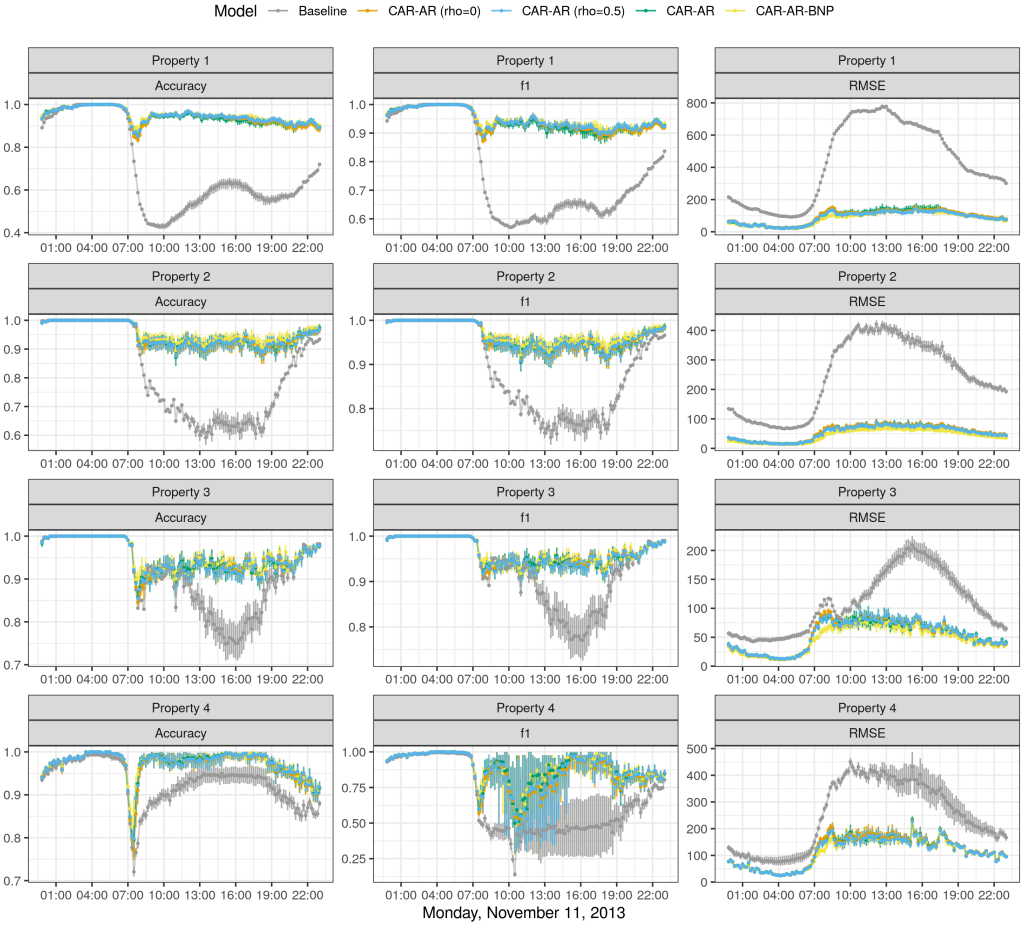


Fig. 6. Mean accuracy, F1 score for the Bayesian predictive satisfaction measure and the RMSE of the robustness measure (points) with their corresponding 80% credible intervals for a rolling window exercise.

Finally, we also investigate the performance of the five models in terms of the predictive measures based on property satisfaction and robustness introduced in Section 3.2. The property parameters used for all properties are $c = 500$, $h_{P,1} = h_{P,3} = 30$ min, $h_{P,2} = 10$ min, $h_{P,4} = 40$ min, $d_{P,2} = d_{P,3} = 1$ cell, $d_{P,4} = 4$ cells. Table 1 shows the posterior mean and standard deviation of the satisfaction accuracy, satisfaction F1 score and robustness RMSE for all four properties. We observe that the CAR-AR-BNP model is the best-performing one in terms of the measures inspected, however, the difference in performance for some properties is not large. Figure 6 presents the average value of the measures in Table 1 for all testing periods, together with 80% credible intervals. This figure can be used for deciding which model performs best in terms of specific interest in the verified properties. For example, it can be seen that the autoregressive models perform similarly in terms of satisfaction measures for all properties, while the robustness of the model CAR-AR-BNP is better for properties P.2 and P.3. The same model also outperforms the others in terms of property P.4 during the rush hours 07:00–09:00, so it should be chosen if the performance in this specific time frame is of interest to the modeler.

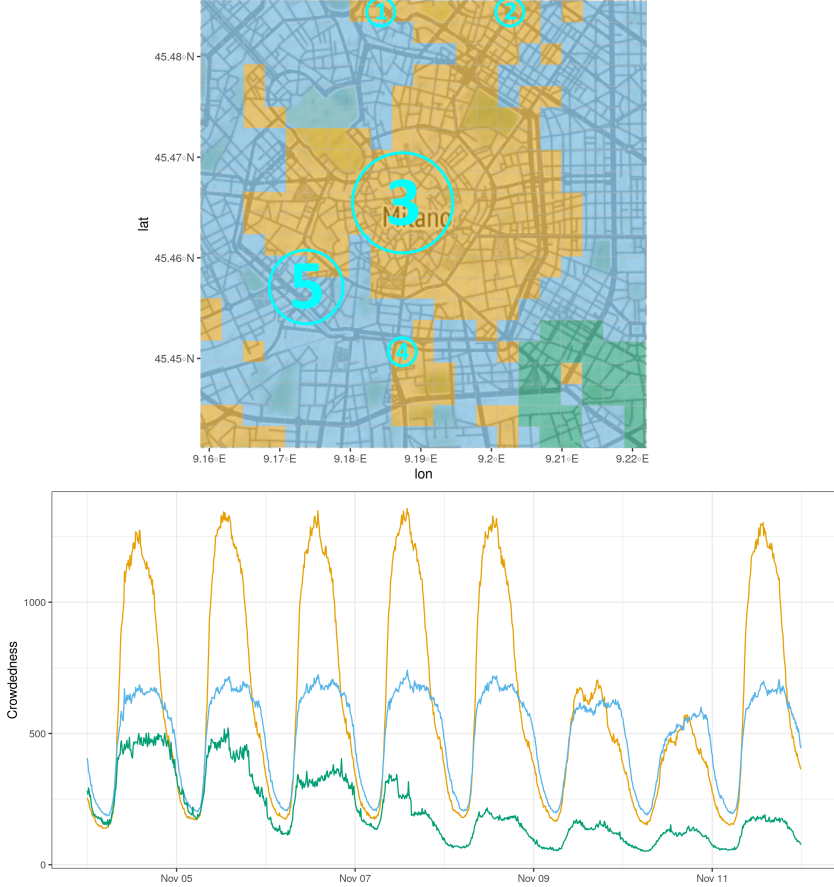


Fig. 7. Top panel: Clusters as identified by Binder's loss. Bottom panel: crowdedness measure averaged over all locations in one cluster. The marked areas in the top panel represent: (1) Garibaldi Station, (2) Central Station, (3) Duomo, (4) Bocconi, (5) Navigli.

4.3 Results of the spatio-temporal model with spatial clustering

We present in the following the results of the CAR-AR-BNP model. The top panel in Figure 7 presents the three clusters identified by employing Binder's loss on the samples of the cluster assignments vector, while the bottom panel presents the crowdedness measure averaged over all locations in one cluster. The blue cluster is one where the difference in the crowdedness between weekends and working days is not as large as for the other two, with activity peaking in the morning (stronger during the working days) as well as in the evening (stronger effect on Sunday). The (5) Navigli area is a member of the blue cluster. The yellow cluster contains areas where the activity is high on the working days and lower on the weekends, with an intraday peak around noon. Typical locations in this cluster are university centers or the city center, where most office buildings are situated. The green cluster is the smallest one, with the characteristic that the activity plummets during the weekend. The area corresponding to this cluster is Porta Romana, which contains the train station with the same name, a station primarily used by commuters into the city.

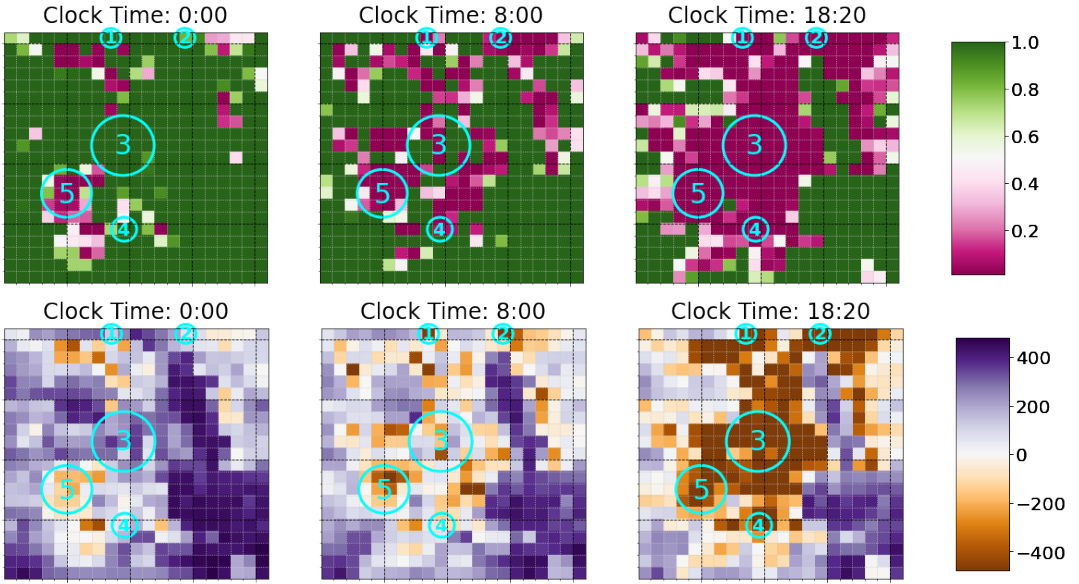


Fig. 8. Posterior satisfaction probability (top row) and posterior mean of the robustness measure (bottom row) resulting from checking for property P.1 at three times of the day. The marked areas represent: (1) Garibaldi Station, (2) Central Station, (3) Duomo, (4) Bocconi, (5) Navigli.

Moreover, the rather isolated areas belonging to one cluster but enclosed by areas in other clusters seem to be explainable and likely not caused by model artifacts. For example, the yellow square in the middle of the green cluster is the location of a large shopping mall.

Finally, posterior means of the parameters that measure time and space dependence indicate strong persistence in both space and time.

4.4 Verification of the crowdedness requirements for spatio-temporal model with spatial clustering

4.4.1 P.1 – Overloads are temporary. Figure 8 shows the estimated posterior satisfaction probability and the posterior mean of the robustness measure resulting from the evaluation of property P.1. Note that P.1 defines a property only in terms of a temporal operator, where we set $h_{P.1} = 30$ min. That is, we check whether the crowdedness variable stays below a value of $c = 500$ or, in case it exceeds this value, then it must return below it within 30 minutes. When looking at the results, it appears clear that the city is roughly split into two macro-areas: the historical and financial center is unlikely to satisfy the property during busy times, while the residential areas are almost always satisfying it. A relevant exception comes from the (5) Navigli area (left bottom of the map): it is, in fact, a vibrant area, where many young people live, which has many touristic landmarks and an active commercial area. We can see that this area is consistently violating our requirement over time, although, from a look at the robustness its actual value is close to zero, meaning that the violation is quite small, making it less concerning from a network capacity perspective.

4.4.2 P.2 – Overloads are local. Figure 9 shows the estimated posterior satisfaction probability and the posterior mean of the robustness measure resulting from the evaluation of property P.2 at three different times of the day. Note that this property is based only on predictions of neighboring

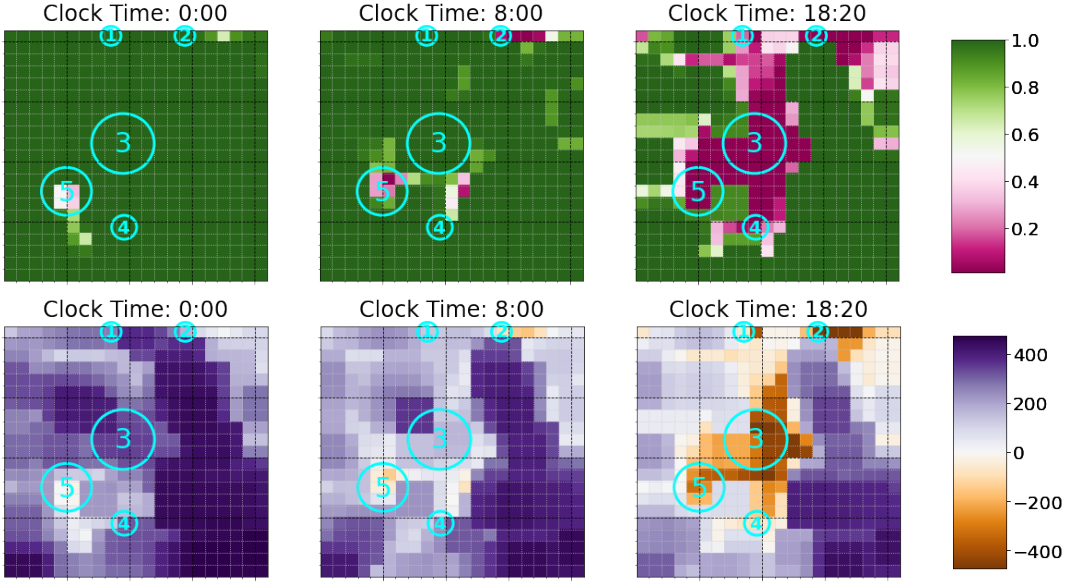


Fig. 9. Posterior satisfaction probability (top row) and posterior mean of the robustness measure (bottom row) resulting from checking property P.2 at three times of the day. The marked areas represent: (1) Garibaldi Station, (2) Central Station, (3) Duomo, (4) Bocconi, (5) Navigli.

locations ($d_{P,2} = 1$ cell) at future time $t + h_{P,2}$, with $h_{P,2} = 10$ min. As one might intuitively expect, the property exhibits high values of satisfaction and robustness for a large area of the city center (there is usually at least an uncrowded area connected to a crowded one). A notable exception is the (3) Duomo area, from which crowds spread towards the other hot spots at the busiest time of the day (18:20). However, by looking at the posterior predictive mean of the robustness for different time points, we get a clearer understanding of the spatial distribution of the excessive loads. In fact, it is evident that the (3) Duomo is the area that might most likely suffer from excessive crowdedness, without any possibility of enacting load-balancing strategies based on the state of nearby locations. Conversely, other areas, like the (5) Navigli area, have a much safer spatial behavior, either because they exceed the threshold only slightly, or because they are surrounded by areas with much lower levels of crowdedness.

4.4.3 P.3 – The network is fault-tolerant. Figure 10 shows the estimated posterior satisfaction probability and the posterior mean of the robustness measure resulting from the evaluation of property P.3 at three different times of the day. Property P.3 enforces the availability of a neighboring uncrowded area (i.e., $d_{P,3} = 1$) consistently for $h_{P,3} = 30$ min. The first thing the reader might notice is that this property exhibits a visual pattern similar to P.1–P.2, except that it is in general less likely to be satisfied. This behavior is to be expected, as one can notice when looking at the logic formulas: P.3 resembles, in fact, the structure of the right side of implication (“ \rightarrow ”) in P.1–P.2, except that it enforces stricter requirements (there must be an uncrowded area for the next half-hour). This observation shows a key strength of logic for the validation and explainability of specifications: from an informal perspective, P.1 and P.2 describe different aspects than P.3. Yet, the obtained results show that P.3 could effectively replace P.1–P.2 as a specification that encompasses both of them. In fact, P.3 summarizes the ideal behavior of a fault-tolerant system overall. Verifying this

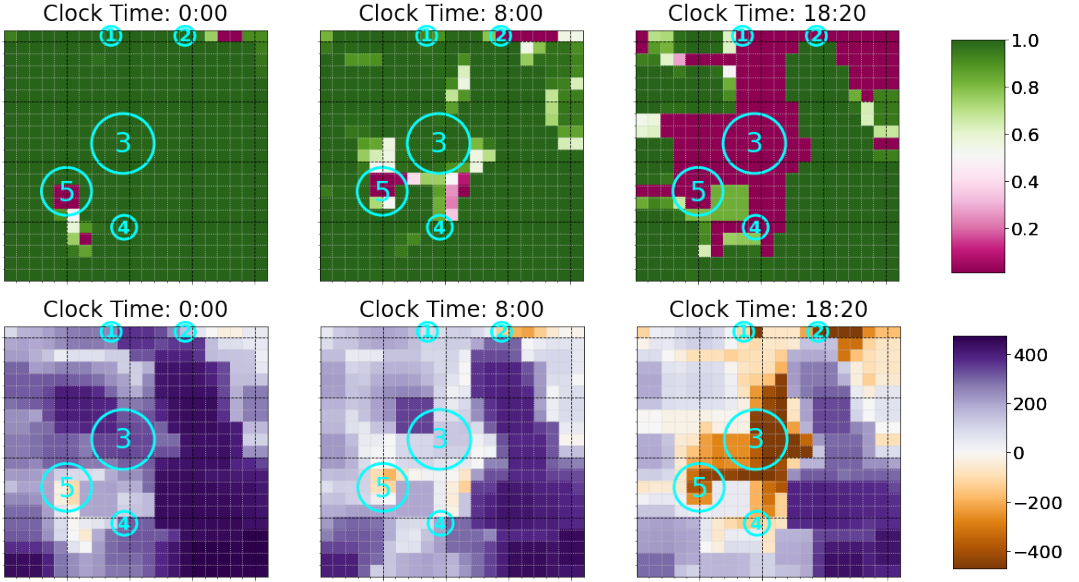


Fig. 10. Posterior satisfaction probability (top row) and posterior mean of the robustness measure (bottom row) resulting from checking property P.3 at three times of the day. The marked areas represent: (1) *Garibaldi Station*, (2) *Central Station*, (3) *Duomo*, (4) *Bocconi*, (5) *Navigli*.

property clearly shows that the city is split into two parts, with the most-touristic part less likely to satisfy the property, while the residential and non-touristic areas are more likely to satisfy it.

4.4.4 P.4 – Uncrowded reachability. Figure 11 presents the results of verifying property P.4 for $h_{P.4} = 40\text{min}$ and $d_{P.4} = 4$ cells (approximately 1 km). (H) circles mark hospitals' locations, where the property is trivially satisfied in all circumstances. By looking at the picture, an immediate observation is that areas at the corners are simply too far from any of the city center hospitals, meaning that going towards the center from there would be impractical. However, it is interesting to see that, while it is never very easy to get to hospitals in busy times (like at 18:20), the (2) *Central Station* is still in a good spot (as it is not too far, and not too crowded), conversely the (1) *Garibaldi Station* is in a less favorable location, as it becomes practically inaccessible in crowded times. Even worse is the (3) *Duomo* area, which, despite being quite close to a hospital, experiences such high levels of crowdedness that make reaching the hospital almost impossible in crowded times (in terms of the requirement we have defined), while it is relatively easier in medium-crowded times. Lastly, the always failing areas at the corners of the grid, and at the bottom-center tell us something different: for the spatial configuration we are considering, they always violate the requirement to reach a hospital in the city center in $d_{P.4}$. This can be surprising at first, but a look at the broader map of the city clarifies that they are closer to hospitals that are not in our grid and, therefore cannot be fully analyzed by our model.

5 DISCUSSION AND FUTURE WORK

In this paper, we propose a framework for predictive model checking and comparison, where in addition to usual approaches, we advocate for the specification of concrete (spatio-temporal)

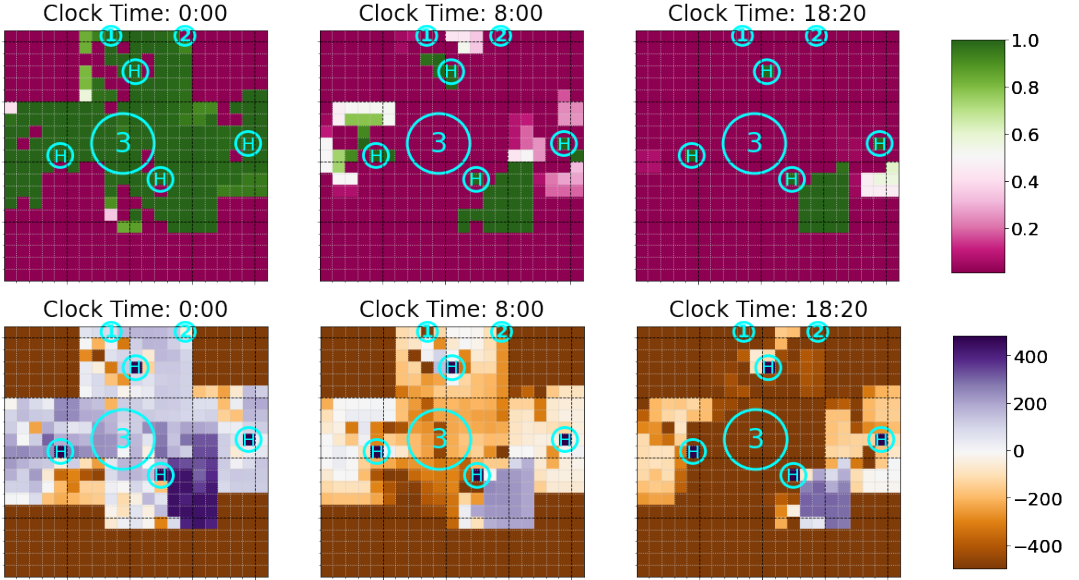


Fig. 11. Posterior satisfaction probability (top row) and posterior mean of the robustness measure (bottom row) resulting from monitoring the property P.4 at three times of the day. The marked areas represent: (1) Garibaldi Station, (2) Central Station, (3) Duomo.

properties that the predictions from a model should satisfy. Given trajectories from the Bayesian predictive distribution, the posterior predictive probability of satisfaction and the posterior predictive robustness of these properties can be approximated by verifying the properties on each of the trajectories efficiently using techniques from formal verification methods. Finally, we can evaluate ex post the model by comparing the resulting measures with the values in the observed data.

We illustrate the approach by building a Bayesian spatio-temporal model for areal crowdedness extracted from aggregated mobile phone data in the city of Milan and by formulating properties that the crowdedness level in the city network should satisfy in order to robustly withstand critical events. We compare various model specifications which include a harmonic regression with and without random effects, as well as a model which performs clustering of the area-specific harmonic regression coefficients. The model that performs clustering is indeed the one that performs best in terms of the proposed measures. This model can however be further refined to clustering over time or a temporal evolution of the persistence parameter for the autoregressive random effects.

The proposed framework advocates for exploiting the rich information that Bayesian predictive inference offers in the form of draws from the posterior predictive distribution of future values, by evaluating models also based on properties that can be directly translated into decision-making. Therefore, we showcase how different model specifications are then evaluated based on well-known performance measures but also on posterior predictive measures employed in formal verification, such as the satisfaction probabilities or the robustness measure.

On a larger scale, by exploiting the synergy between Bayesian modeling and formal verification methods, we also advocate for the development and use of explainable algorithms where properties relevant to decision-making are incorporated into the data analytic process flow. Therefore, the proposed approach has a clear potential in the area of sustainable cities and urban mobility, as these applications deal with complex systems, with a multitude of stakeholders and with a pressing

need for transparency in the decision-making process. We hope for the illustration in the current paper to open the way to further applications.

Computational details and replication materials. The computations have been performed on 25 IBM dx360M3 nodes within a cluster of workstations. Instruction for downloading the data set as well as an extensive description can be found in [2]. The estimation of the Bayesian models can be performed using code in the repository at <https://github.com/lauravana/CARBayesSTBNP>. The Moonlight tool is available at <https://github.com/moonlightsuite/moonlight>, while the specific problem instance related to this project, together with the data and the scripts for generating the figures, are available at <https://github.com/ennioVisco/bayesformal>.

REFERENCES

- [1] Sudipto Banerjee. 2017. High-dimensional Bayesian geostatistics. *Bayesian Analysis* 12, 2 (2017), 583 – 614. <https://doi.org/10.1214/17-BA1056R>
- [2] Gianni Barlacchi, Marco De Nadai, Roberto Larcher, Antonio Casella, Cristiana Chitic, Giovanni Torrisi, Fabrizio Antonelli, Alessandro Vespiagnani, Alex Pentland, and Bruno Lepri. 2015. A multi-source dataset of urban life in the city of Milan and the Province of Trentino. *Scientific data* 2, 1 (2015), 1–15. <https://doi.org/10.1038/sdata.2015.55>
- [3] Alba Bernini, Amadou Lamine Toure, and Renato Casagrandi. 2019. The time varying network of urban space uses in Milan. *Applied Network Science* 4, 1 (2019), 1–16. <https://doi.org/10.1007/s41109-019-0245-x>
- [4] Pietro Bonato, Paolo Cintia, Francesco Fabbri, Daniele Fadda, Fosca Giannotti, Pier Luigi Lopalco, Sara Mazzilli, Mirco Nanni, Luca Pappalardo, Dino Pedreschi, Francesco Penone, Salvatore Rinzivillo, Giulio Rossetti, Marcello Savarese, and Lara Tavoschi. 2020. Mobile phone data analytics against the COVID-19 epidemics in Italy: flow diversity and local job markets during the national lockdown. *CoRR* abs/2004.11278 (2020), 24 pages. arXiv:[2004.11278](https://arxiv.org/abs/2004.11278) <https://arxiv.org/abs/2004.11278>
- [5] Luca Bortolussi, Francesca Cairoli, Ginevra Carbone, and Paolo Pulcini. 2023. Scalable Stochastic Parametric Verification with Stochastic Variational Smoothed Model Checking. In *Runtime Verification - 23rd International Conference, RV 2023, Thessaloniki, Greece, October 3–6, 2023, Proceedings (Lecture Notes in Computer Science, Vol. 14245)*, Panagiotis Katsaros and Laura Nenzi (Eds.). Springer, 45–65. https://doi.org/10.1007/978-3-031-44267-4_3
- [6] Luca Bortolussi, Dimitrios Milios, and Guido Sanguinetti. 2016. Smoothed model checking for uncertain Continuous-Time Markov Chains. *Inf. Comput.* 247 (2016), 235–253. <https://doi.org/10.1016/J.IC.2016.01.004>
- [7] Luca Bortolussi and Simone Silvetti. 2018. Bayesian Statistical Parameter Synthesis for Linear Temporal Properties of Stochastic Models. 10806 (2018), 396–413. https://doi.org/10.1007/978-3-319-89963-3_23
- [8] Annalisa Cadonna, Andrea Cremaschi, and Alessandra Guglielmi. 2019. Bayesian modeling for large spatio-temporal data: an application to mobile networks. In *Smart Statistics for Smart Applications. Book of Short Papers SIS 2019*. Pearson, Società Italiana di Statistica, Università Cattolica del Sacro Cuore, Largo Gemelli 1, 691–696.
- [9] Jonathan Cinnamon, Sarah K Jones, and W Neil Adger. 2016. Evidence and future potential of mobile phone data for disease disaster management. *Geoforum* 75 (2016), 253–264. <https://doi.org/10.1016/j.geoforum.2016.07.019>
- [10] Edmund M. Clarke and E. Allen Emerson. 1982. Design and synthesis of synchronization skeletons using branching time temporal logic. In *Logics of Programs*, Dexter Kozen (Ed.). Springer Berlin Heidelberg, Berlin, Heidelberg, 52–71.
- [11] Pierre Deville, Catherine Linard, Samuel Martin, Marius Gilbert, Forrest R Stevens, Andrea E Gaughan, Vincent D Blondel, and Andrew J Tatem. 2014. Dynamic population mapping using mobile phone data. *Proceedings of the National Academy of Sciences* 111, 45 (2014), 15888–15893. <https://doi.org/10.1073/pnas.1408439111>
- [12] Georgios E. Fainekos and George J. Pappas. 2009. Robustness of temporal logic specifications for continuous-time signals. *Theoretical Computer Science* 410, 42 (2009), 4262–4291. <https://doi.org/10.1016/j.tcs.2009.06.021>
- [13] Stefano Favaro and Yee Whye Teh. 2013. MCMC for normalized random measure mixture models. *Statist. Sci.* 28, 3 (2013), 335–359. <https://doi.org/10.1214/13-STS422>
- [14] Claudio Gariazzo, Armando Pelliccioni, and Maria Paola Bogliolo. 2019. Spatiotemporal analysis of urban mobility using aggregate mobile phone derived presence and demographic data: a case study in the city of Rome, Italy. *Data* 4, 1 (2019), 25 pages. <https://doi.org/10.3390/data4010008>
- [15] Andrew Gelman, Xiao-Li Meng, and Hal Stern. 1996. POSTERIOR PREDICTIVE ASSESSMENT OF MODEL FITNESS VIA REALIZED DISCREPANCIES. *Statistica Sinica* 6, 4 (1996), 733–760. <http://www.jstor.org/stable/24306036>
- [16] John Geweke and Gianni Amisano. 2010. Comparing and evaluating Bayesian predictive distributions of asset returns. *International Journal of Forecasting* 26, 2 (2010), 216–230. <https://doi.org/10.1016/j.ijforecast.2009.10.007>
- [17] Tilmann Gneiting and Adrian E Raftery. 2007. Strictly proper scoring rules, prediction, and estimation. *J. Amer. Statist. Assoc.* 102, 477 (2007), 359–378. <https://doi.org/10.1198/016214506000001437>

- [18] Md Shahadat Iqbal, Charisma F Choudhury, Pu Wang, and Marta C González. 2014. Development of origin–destination matrices using mobile phone call data. *Transportation Research Part C: Emerging Technologies* 40 (2014), 63–74. <https://doi.org/10.1016/j.trc.2014.01.002>
- [19] Gregor Kastner. 2016. Dealing with stochastic volatility in time series using the R package stochvol. *Journal of Statistical Software* 69, 5 (2016), 1–30. <https://doi.org/10.18637/jss.v069.i05>
- [20] Leonhard Knorr-Held and Håvard Rue. 2002. On block updating in Markov random field models for disease mapping. *Scandinavian Journal of Statistics* 29, 4 (2002), 597–614. <https://doi.org/10.1111/1467-9469.00308>
- [21] Fabian Krüger, Sebastian Lerch, Thordis Thorarinsdottir, and Tilmann Gneiting. 2021. Predictive inference based on Markov chain Monte Carlo output. *International Statistical Review* 89, 2 (2021), 274–301. <https://doi.org/10.1111/insr.12405>
- [22] Axel Legay, Anna Lukina, Louis Marie Traonouez, Junxing Yang, Scott A. Smolka, and Radu Grosu. 2019. *Statistical Model Checking*. Springer International Publishing, Cham, 478–504. https://doi.org/10.1007/978-3-319-91908-9_23
- [23] Brian G. Leroux, Xingye Lei, and Norman Breslow. 2000. Estimation of Disease Rates in Small Areas: A new Mixed Model for Spatial Dependence. In *Statistical Models in Epidemiology, the Environment, and Clinical Trials*, M. Elizabeth Halloran and Donald Berry (Eds.). Springer New York, New York, NY, 179–191.
- [24] James E. Matheson and Robert L. Winkler. 1976. Scoring rules for continuous probability distributions. *Management Science* 22, 10 (1976), 1087–1096. <https://doi.org/10.1287/mnsc.22.10.1087>
- [25] William J McCausland, Shirley Miller, and Denis Pelletier. 2011. Simulation smoothing for state-space models: A computational efficiency analysis. *Computational Statistics & Data Analysis* 55, 1 (2011), 199–212. <https://doi.org/10.1016/j.csda.2010.07.009>
- [26] Alexander Mozdzen, Andrea Cremaschi, Annalisa Cadonna, Alessandra Guglielmi, and Gregor Kastner. 2022. Bayesian modeling and clustering for spatio-temporal areal data: An application to Italian unemployment. *Spatial Statistics* 52 (2022), 100715. <https://doi.org/10.1016/j.spasta.2022.100715>
- [27] Laura Nenzi, Ezio Bartocci, Luca Bortolussi, and Michele Loreti. 2022. A Logic for Monitoring Dynamic Networks of Spatially-distributed Cyber-Physical Systems. *Log. Methods Comput. Sci.* 18, 1 (2022). [https://doi.org/10.46298/LMCS-18\(1:4\)2022](https://doi.org/10.46298/LMCS-18(1:4)2022)
- [28] Laura Nenzi, Ezio Bartocci, Luca Bortolussi, Michele Loreti, and Ennio Visconti. 2020. Monitoring spatio-temporal properties. In *Runtime Verification*, Jyotirmoy Deshmukh and Dejan Ničković (Eds.). Springer International Publishing, Cham, 21–46.
- [29] Laura Nenzi, Ezio Bartocci, Luca Bortolussi, Simone Silvetti, and Michele Loreti. 2023. MoonLight: a lightweight tool for monitoring spatio-temporal properties. *Int. J. Softw. Tools Technol. Transf.* 25, 4 (2023), 503–517. <https://doi.org/10.1007/S10009-023-00710-5>
- [30] Laura Nenzi, Luca Bortolussi, Vincenzo Ciancia, Michele Loreti, and Mieke Massink. 2017. Qualitative and quantitative monitoring of spatio-temporal properties with SSTL. *arXiv preprint arXiv:1706.09334 abs/1706.09334* (2017), 38 pages. [https://doi.org/10.23638/LMCS-14\(4:2\)2018](https://doi.org/10.23638/LMCS-14(4:2)2018)
- [31] Jan Peters-Anders, Zaheer Khan, Wolfgang Loibl, Helmut Augustin, and Arno Breinbauer. 2017. Dynamic, interactive and visual analysis of population distribution and mobility dynamics in an urban environment using the mobility explorer framework. *Information* 8, 2 (2017), 56. <https://doi.org/10.3390/info8020056>
- [32] J. P. Queille and J. Sifakis. 1982. Specification and verification of concurrent systems in CESAR. In *International Symposium on Programming*, Mariangiola Dezani-Ciancaglini and Ugo Montanari (Eds.). Springer Berlin Heidelberg, Berlin, Heidelberg, 337–351.
- [33] Terrance D. Savitsky and Matthew R. Williams. 2022. Bayesian dependent functional mixture estimation for area and time-indexed data: an application for the prediction of monthly county employment. *Bayesian Analysis* 17, 3 (2022), 791 – 815. <https://doi.org/10.1214/21-BA1274>
- [34] Zhensheng Wang, Yang Yue, Biao He, Ke Nie, Wei Tu, Qingyun Du, and Qingquan Li. 2021. A Bayesian spatio-temporal model to analyzing the stability of patterns of population distribution in an urban space using mobile phone data. *International Journal of Geographical Information Science* 35, 1 (2021), 116–134. <https://doi.org/10.1080/13658816.2020.1798967>
- [35] NA Wardrop, WC Jochem, TJ Bird, HR Chamberlain, D Clarke, D Kerr, L Bengtsson, S Juran, V Seaman, and AJ Tatem. 2018. Spatially disaggregated population estimates in the absence of national population and housing census data. *Proceedings of the National Academy of Sciences* 115, 14 (2018), 3529–3537. <https://doi.org/10.1073/pnas.1715305115>
- [36] Håkan L. S. Younes, Marta Kwiatkowska, Gethin Norman, and David Parker. 2006. Numerical vs. statistical probabilistic model checking. *International Journal on Software Tools for Technology Transfer* 8, 3 (June 2006), 216–228. <https://doi.org/10.1007/s10009-005-0187-8>
- [37] Paolo Zuliani, André Platzer, and Edmund M Clarke. 2013. Bayesian statistical model checking with application to Stateflow/Simulink verification. *Formal Methods in System Design* 43, 2 (2013), 338–367. <https://doi.org/10.1007/s10703-013-0195-3>

ACKNOWLEDGMENTS

The authors acknowledge funding from the Austrian Science Fund (FWF) for the project “High-dimensional statistical learning: New methods to advance economic and sustainability policies” (ZK 35), jointly carried out by the University of Klagenfurt, the University of Salzburg, TU Wien, and the Austrian Institute of Economic Research (WIFO).

Appendix A MODELS

Baseline model. The simplest model considered is a harmonic regression, where we assume that the dependence in crowdedness is explained by the harmonic regressors and with error term $\eta_{i,t} \stackrel{iid}{\sim} \mathcal{N}(0, \sigma^2)$. Moreover, we assume that all spatial units share the same temporal behavior with $\beta_i \equiv \beta$.

CAR-AR models with common harmonic regression coefficients. The error term $\eta_{i,t}$ is split into two components:

$$\eta_{i,t} = w_{i,t} + \epsilon_{i,t},$$

where $\epsilon_{i,t}$ is normally distributed $\epsilon_{i,t} \stackrel{iid}{\sim} \mathcal{N}(0, \sigma^2)$ and $w_{i,t}$ is a space-time random effect that captures the spatio-temporal dependence in the log crowdedness measure unexplained by the Fourier covariates. The random effect $w_{i,t}$ is modeled as a stationary first-order autoregressive process:

$$w_{i,t} = \xi w_{i,t-1} + \sqrt{1 - \xi^2} u_{i,t}, \quad t = 2, \dots, T, \quad (7)$$

where $\xi \in (-1, 1)$ to ensure stationarity of the model and $u_{i,t}$ is a mean zero stationary spatial innovation process with variance τ^2 which is independent over time but correlated over the spatial units:

$$u_t \stackrel{iid}{\sim} \mathcal{N}(\mathbf{0}, \tau^2 Q(\rho, W)^{-1}).$$

For the first time point we have $w_1 \sim \mathcal{N}(\mathbf{0}, \tau^2 Q(\rho, W)^{-1})$. The matrix $Q(\rho, W)$ denotes the spatial precision proposed in [23]:

$$Q(\rho, W) = \rho(\text{diag}(W\mathbf{1}) - W) + (1 - \rho)\mathbb{I},$$

where $\mathbf{1}$ is the $I \times 1$ vector of ones, while \mathbb{I} is the $I \times I$ identity matrix. In this spatial prior, $0 \leq \rho \leq 1$ provides a measure of spatial dependence while the spatial auto-correlation is controlled by the symmetric $I \times I$ adjacency matrix W , where w_{kl} is equal to one if area k shares an edge or a vertex with area l and zero otherwise (the so-called queen contiguity). This mean-zero normal prior on the spatial innovations is referred to in the literature as a spatial conditionally autoregressive (CAR) prior. We assume again one common set of regression coefficients $\beta_i \equiv \beta$.

CAR-AR model with spatial clustering (CAR-AR-BNP). We modify the model introduced above in order to identify areas with similar seasonality patterns. We place a Bayesian non-parametric (BNP) Dirichlet process prior to the β_i coefficients for all locations:

$$\beta_i | P \stackrel{iid}{\sim} P, \quad i = 1, \dots, I, \text{ with } P \sim \text{DP}(\alpha, P^0), \quad P(\cdot) = \sum_{j=1}^{\infty} \pi_j \delta_{\theta_j}(\cdot), \quad (8)$$

where the random measure P is represented as the infinite sum of the product of random weights π_j and locations $\theta_j \sim P^0$ and δ_θ represents the point mass at θ . The stick-breaking prior is assumed on the common weights $\pi_j / \prod_{i=1}^{j-1} (1 - \pi_i) \sim \text{Beta}(1, \alpha)$ and the reference measure is specified as $P^0(\beta) = \mathcal{N}_{2K}(\beta | \mathbf{m}_0, S_0)$.

Further priors and estimation. The intercept term β_0 has a mean zero normal prior. For the models with one set of regression coefficients, we employ $\beta \sim \mathcal{N}_{2K}(\beta | \mathbf{m}_0, S_0)$. Uniform priors are set on ρ and ξ and inverse Gamma conjugate priors are set for the variance parameters: $\sigma^2 \sim \text{IG}(a^\sigma, b^\sigma)$ and $\tau^2 \sim \text{IG}(a^\tau, b^\tau)$. These component specifications, along with our apriori independence assumption, form the joint prior.

Inference is performed using MCMC methods. The CAR-AR models are Gaussian state space models where the full conditional distributions of the parameters have a closed form, so a Gibbs sampler can be employed. A rough outline of the samplers is given below:

- (1) For CAR-AR-BNP: The marginalized sampler together with the reuse algorithm in [13] is implemented for sampling the cluster assignments and the unique values of the cluster parameters [cf. 8, 26].
- (2) The unique values of the regression coefficients are sampled from the full conditional.
- (3) To sample the spatio-temporal random effects $w_{i,t}$ efficiently from an $I \times T$ multivariate normal distribution, we exploit the sparsity of the spatial precision matrix [cf. 1, 20, 25].
- (4) Parameters ρ and ξ are sampled from a truncated normal distribution on the intervals $[0, 1]$ and $[-1, 1]$, respectively.
- (5) Variance parameters τ^2 and σ^2 are sampled from the respective conjugate full conditional posterior distribution.

For all models, the values of the hyperparameters are kept identical: $\mathbf{m}_0 = \mathbf{0}$, $S_0 = 0.1\mathbb{I}_{2K}$, $a^\sigma = a^\tau = 1$, $b^\sigma = b^\tau = 0.01$. We take $\alpha = 1$ in the BNP prior, and we use $C = 50$ auxiliary variables in the algorithm for sampling the cluster assignments [see Section 3.2.1 in 13].